Dalton Transactions

Understanding gate adsorption behaviour of CO_2 on elastic layer-structured metal-organic framework-11

Journal:	*Dalton Transactions*
Manuscript ID	DT-ART-09-2015-003476.R1
Article Type:	Paper
Date Submitted by the Author:	08-Oct-2015
Complete List of Authors:	Hiraide, Shotaro; Kyoto University, Department of Chemical Engineering Tanaka, Hideki; Kyoto University, Department of Chemical Engineering Miyahara, Minoru; Kyoto University, Department of Chemical Engineering

Dalton Transactions

ARTICLE

Understanding gate adsorption behaviour of CO_2 on elastic layer-structured metal-organic framework-11

Received 00th January 20xx,
Accepted 00th January 20xx

DOI: 10.1039/x0xx00000x

www.rsc.org/

Shotaro Hiraide, Hideki Tanaka* and Minoru T. Miyahara*

We demonstrate that CO_2 gate adsorption behaviour of elastic layer-structured metal-organic framework-11 (ELM-11: $[Cu(BF_4)_2(4,4'\text{-bipyridine})_2]$), which is a family of soft porous crystals (SPCs), can be described by a thermodynamic model by free energy analysis with the aid of an adsorption experiment and a molecular simulation. The structure of ELM-11 (closed structure) at 273 K after its evacuation and CO_2-encapsulated ELM-11 (open structure) at 195–298 K were determined by the Rietveld analysis using in situ synchrotron X-ray powder diffraction data. We then performed grand canonical Monte Carlo (GCMC) simulations for CO_2 adsorption on the open host framework structures of ELM-11 from the Rietveld analysis. The temperature dependence of the Helmholtz free energy change of host ΔF^{host} from the closed structure to the open structure was obtained by the free energy analysis using the GCMC data. We show that there is a linear correlation between ΔF^{host} and temperature, and thus, the internal energy and entropy changes of host, ΔU^{host} and ΔS^{host}, respectively, can be obtained. The obtained ΔU^{host} value is in good agreement with that obtained from the quantum chemical calculations using the closed and open host framework structures, which demonstrates that the thermodynamic model for gate adsorption is highly appropriate. Moreover, our result suggests that the gate adsorption pressure depends on not only the guest-host interaction and the internal energy change of host, but also the entropy change of host, which should be one of the key factors for the tailored synthesis of SPCs.

Introduction

Metal-organic frameworks (MOFs) or porous coordination polymers (PCPs) are a new class of materials assembled with metal ions and organic linkers.[1-6] Various combinations of metal ions and organic linkers enable molecular-level control of the pore size for specific gas storage and separation systems. In particular, third-generation PCPs classified by Kitagawa and co-workers,[3,7,8] the so-called soft porous crystals (SPCs),[9] have attracted much attention because of their unique properties: SPCs exhibit structural deformations in response to various external stimuli such as temperature change, pressurization, and guest adsorption.[8-10] The adsorption-induced structural transition of SPCs, referred to as 'gate adsorption' or 'breathing', leads to a steep rise in the adsorption isotherm at a threshold gas pressure, which will open new possibilities for highly efficient gas storage (large amount of deliverable gas) and separation processes (large selectivity by molecular recognition) in the chemical industry. However, at present, the rational design of SPCs tailored to specific chemical unit operations is still a challenging task, requiring extensive experiment-based screening to optimize the desired properties. Therefore, sophisticated thermodynamic modelling of gate adsorption is required to find suitable existing SPCs and/or to design new SPCs with desirable performance.

A thermodynamic model on the basis of free energy analysis is promising to describe the gate adsorption. Coudert *et al.*[11] first developed a thermodynamic expression for gate adsorption behaviour based on the osmotic statistical ensemble, and proposed an analytical method for estimating the Helmholtz free energy change of host framework ΔF^{host} due to a structural transition by fitting a Langmuir isotherm to a plateau region of the experimental isotherm after the gate adsorption. The temperature–pressure phase diagram of Xe adsorption on MIL-53[12] and a binary mixture of CH_4 and CO_2 on MIL-53[13] were then predicted with good accuracy by using this approach. Neimark *et al.* developed a thermodynamic description incorporating the adsorption-induced stress exerted on SPCs, and successfully explained the hysteresis phenomenon experimentally observed for the breathing transitions in Xe–MIL-53[14] and CO_2–MIL-53[15] systems.

Watanabe *et al.* applied molecular simulations to free energy analysis.[16] They performed grand canonical Monte

Department of Chemical Engineering, Kyoto University, Nishikyo, Kyoto 615-8510, Japan.
*E-mail: tanaka@cheme.kyoto-u.ac.jp, miyahara@cheme.kyoto-u.ac.jp.
†Electronic Supplementary Information (ESI) available: interaction parameters for a CO_2 molecule; Rietveld refinement patterns, snapshots, and atomic coordinates of ELM-11 ⊃ $2CO_2$ at 195 – 298 K; Le Bail fitting patterns of ELM-11 at 195 – 298 K; atomic coordinates of ELM-11 at 273 K; atomic charges from the Mulliken population analysis for the open framework of ELM-11; snapshot of CO_2 configuration at a low temperature and high pressure by GCMC; bond distances of ELM-11 and ELM-11 ⊃ $2CO_2$ structures before and after the geometry optimization by DFT-D; Rietveld refinement patterns (only profile fitting) of ELM-11 and ELM-11 ⊃ $2CO_2$ at 273 K using the optimized structures by DFT-D as the initial structures; fictitious adsorption isotherm of CO_2 on the optimized framework at 273 K; details of the newly developed structure refinement method by which the closed structure of ELM-11 was determined. See DOI: 10.1039/x0xx00000x

Carlo (GCMC) simulations for a simple toy model of mutually interpenetrating jungle-gym (JG) framework structures, and calculated the free energy landscape by integrating a force exerted against a JG framework by adsorbates. The free energy landscape revealed the existence of an energy barrier between the stabilized and metastabilized states on a transition coordinate, which helped explain the hysteresis phenomenon. Their methodology was successfully applied to various simple toy models such as interpenetrating JG,[17] stacked-layer,[18-20] and lozenge-shaped[21,22] motifs.

The thermodynamic model based on free energy analysis has provided a good understanding of the gate adsorption behaviour on simple toy models for SPCs. The next challenge is to quantitatively substantiate that the gate adsorption of real SPCs can be described by using such a thermodynamic model. We have thus performed a free energy analysis in a previous work with the aid of GCMC simulations for the Ar–ZIF-8 system and succeeded in predicting the experimental gate adsorption pressures at 71–91 K.[23] Furthermore, quite recently, free energy analysis has been conducted for the elastic layer-structured metal-organic framework-11 (ELM-11), which exhibits a typical gate adsorption behaviour for CO_2 at room temperature.[24] ELM-11 having a 2D square-grid framework $[Cu(BF_4)_2(bpy)_2]$ (bpy = 4,4′-bipyridine) is obtained by the dehydration of $\{[Cu(bpy)(H_2O)_2(BF_4)_2](bpy)\}$ with a 3D interpenetrated framework (pre-ELM-11), and it transforms into ELM-11 $\supset 2CO_2$ by encapsulating two CO_2 molecules per monomer unit [monomer unit: $Cu(BF_4)_2(bpy)_2$] at 273 K. This compound has been well studied[25-36] as the first SPC for which the gate adsorption behaviour of a gas was observed; however, the structures of ELM-11 and ELM-11 $\supset 2CO_2$ were not precisely determined, because only X-ray powder diffraction (XRPD) measurement was available for both compounds. We thus determined the structure of ELM-11 $\supset 2CO_2$ by our new structure refinement method, which combines the Rietveld analysis of in situ synchrotron XRPD data with molecular simulations, and obtained the ΔF^{host} value at 273 K by performing free energy analysis with the aid of GCMC simulations using the host framework structure from the Rietveld analysis. Moreover, we confirmed that experimental gate adsorption pressures at 258–283 K could be predicted with less than 16% error by using the thermodynamic model assuming that the obtained ΔF^{host} value does not depend on temperature. This fact suggests that the thermodynamic model of gate adsorption can describe the behaviour of real SPCs, but our methodology in the previous study still has some inadequacies: the temperature range in which an experimental gate pressure is predicted with high accuracy is limited, because temperature dependence of ΔF^{host} was neglected; and the obtained value of ΔF^{host} has not been confirmed by other methods such as ab initio calculations using the host framework structures before and after the adsorption-induced structural transition.

In this study, we aim to substantiate that the gate adsorption behaviour of real SPCs can be quantitatively described using the thermodynamic model based on free energy analysis by taking into account the temperature dependence of ΔF^{host}. To achieve this, we determine the temperature dependence of ΔF^{host} for CO_2 gate adsorption on ELM-11 over a wide range of temperature and evaluate the internal energy change of the host framework by the following two ways to confirm the validity of the thermodynamic model: one is the free energy analysis with the aid of an adsorption experiment and GCMC simulations using the open framework structures of ELM-11 determined by the Rietveld analysis at several temperatures; and the other is quantum chemical calculations using the closed and open framework structures of ELM-11. The closed framework structure of ELM-11 is determined by our unique structure refinement method using in situ synchrotron XRPD data. To the best of our knowledge, this is the first study to report the detailed crystal structure of ELM-11 in the closed state.

Experimental

CO_2 adsorption

Pre-ELM-11 was purchased from Tokyo Chemical Industry Co., Ltd. The pre-ELM-11 sample was transformed into ELM-11 by heating at 373 K for 10 h under vacuum (<0.1 mPa), and the completion of the transformation was confirmed by in situ synchrotron XRPD measurement. The adsorption isotherms of CO_2 on ELM-11 at 195, 223, 248, 273, and 298 K were measured by a BELSORP-max instrument (Microtrac Bel) and a cryostat equipped with a two-stage Gifford–McMahon refrigerator.[23] The cell temperature was kept within ±0.01 K during the adsorption measurements.

In situ synchrotron XRPD

The pre-ELM-11 sample was sealed in a 0.4 mm diameter soda glass capillary, which was attached to a stainless steel tube using an epoxy adhesive. The sample was evacuated for 10 h at 373 K. In situ synchrotron XRPD patterns of ELM-11 (closed state) and ELM-11 $\supset 2CO_2$ (open state) at 195, 223, 248, 273, and 298 K were measured at the BL02B2 beamline of SPring-8 with a large Debye-Scherrer-type diffractometer.[37] The cell temperature was controlled by a nitrogen gas blower. After the measurements of the closed state of ELM-11, CO_2 gas of 1.0, 5.6, 22, 100, and 100 kPa was introduced into the soda glass capillary using a lab-made gas handling system at 195, 223, 248, 273, and 298 K, respectively. The wavelengths of the incident X-rays at the respective measurements are tabulated in Tables 1 and 2. The capillary was oscillated by 60° to obtain uniform diffraction intensities.

Structural analysis using X-ray powder diffraction data

The ELM-11 $\supset 2CO_2$ structures at 195, 223, 248, and 298 K were refined by the Rietveld method using PDXL (Rigaku Corp., Japan)[38] and RIETAN-FP[39] software packages. We used the ELM-11 $\supset 2CO_2$ structure at 273 K obtained in a previous study[24] as an initial structure model for the Rietveld refinement, and soft constraints for all bond lengths and bond angles were imposed during the refinements. The peak profile was approximated by a split pseudo-Voigt function, and partial

Table 1 Crystal data for ELM-11 ⊃ $2CO_2$ obtained from the Rietveld analysis.

T [K]	195	223	248	273	298
$P(CO_2)$ [kPa]	1.0	5.6	22	100	100
formula	$CuB_2C_{20}N_4H_{16}F_8 \cdot 2CO_2$	$CuB_2C_{20}N_4H_{16}F_8 \cdot 2CO_2$	$CuB_2C_{20}N_4H_{16}F_8 \cdot 2CO_2$	$CuB_2C_{20}N_4H_{16}F_8 \cdot 2CO_2$	$CuB_2C_{20}N_4H_{16}F_8 \cdot 2CO_2$
crystal system	monoclinic	monoclinic	monoclinic	monoclinic	monoclinic
space group	$C2/c$ (No. 15)	$C2/c$ (No. 15)	$C2/c$ (No. 15)	$C2/c$ (No. 15)	$C2/c$ (No. 15)
a [nm]	1.35777(12)	1.35809(10)	1.36184(9)	1.36851(6)	1.37219(9)
b [nm]	1.10853(7)	1.10535(7)	1.10491(6)	1.10446(3)	1.10542(6)
c [nm]	1.85641(14)	1.86021(11)	1.86480(10)	1.87175(6)	1.87532(10)
β [deg]	94.425(5)	94.817(3)	95.194(4)	95.687(3)	95.924(3)
V [nm^3]	2.7858(4)	2.7826(3)	2.7945(3)	2.8157(2)	2.8294(3)
Z	4	4	4	4	4
R_{wp}	0.04127	0.03969	0.03368	0.02316	0.03514
R_P	0.02731	0.02859	0.02480	0.01561	0.02556
R_I	0.07752	0.07934	0.07261	0.04029	0.07531
S	4.042	3.004	2.521	2.353	2.058
d_{layer} [nm]	0.5676	0.5698	0.5729	0.5776	0.5800
$\lambda_{X\text{-}ray}$ [nm]	0.79901	0.79917	0.79917	0.79937	0.79917

Table 2 Crystal data for ELM-11. The data at 195, 223, 248, and 298 K were obtained from the Le Bail analysis, and the data at 273 K were obtained from the Rietveld refinement.

T [K]	195	223	248	273*	298
formula	–	–	–	$CuB_2C_{20}N_4H_{16}F_8$	–
crystal system	monoclinic	monoclinic	monoclinic	monoclinic	monoclinic
space group	$C2/c$ (No. 15)	$C2/c$ (No. 15)	$C2/c$ (No. 15)	$C2/c$ (No. 15)	$C2/c$ (No. 15)
a [nm]	1.23915	1.24031	1.24382	1.24227(8)	1.24775
b [nm]	1.11825	1.11776	1.11987	1.11618(6)	1.11992
c [nm]	1.61074	1.61088	1.61568	1.61420(11)	1.61752
β [deg]	101.052	100.876	100.719	100.534(4)	100.392
V [nm^3]	2.1906	2.1932	2.2112	2.2005(3)	2.2232
Z	–	–	–	4	–
R_{wp}	0.03741	0.03651	0.03385	0.03225	0.03348
R_P	0.02448	0.02482	0.02351	0.02079	0.02325
R_I	0.01827	0.01531	0.01369	0.07284	0.01884
S	1.191	1.151	1.051	3.276	1.032
d_{layer} [nm]	0.4427	0.4438	0.4458	0.4461	0.4483
$\lambda_{X\text{-}ray}$ [nm]	0.79901	0.79901	0.79901	0.79901	0.79901

profile relaxation was applied for the 021, 202, 020, 204, 130, and $13\bar{1}$ reflections.[40] The scattering of hydrogen atoms of bpy were taken into account, but their coordinates were not refined.

The closed structure of ELM-11 at 273 K was determined by a newly developed structure refinement technique based on a previous method.[24] In this method, Monte Carlo-type molecular moves are made until the reliability factor (R_{wp}), which is an index for the agreement between the observed and calculated XRPD patterns, becomes sufficiently small under a potential energy constraint. The R_{wp} value was evaluated after the parameters for the peak profile were only refined using the RIETAN-2000[41] software package (see ESI† for more details). The structure obtained by this method was used as an input for the Rietveld analysis to further refine the closed structure of ELM-11 using the RIETAN-FP software package. The split pseudo-Voigt function was used to describe the peak profile of the calculated XRPD pattern, and the scattering of hydrogen atoms was considered as was done for the structure refinement of ELM-11 ⊃ $2CO_2$. The partial profile relaxation was applied for the 111, $20\bar{2}$, 020, and $20\bar{4}$ reflections.

Grand canonical Monte Carlo simulation

Adsorption isotherms of CO_2 on the open framework structures of ELM-11 at 195–298 K were obtained by the

GCMC method. The Rietveld refined structure at the corresponding temperature was used as the open framework structure for the GCMC simulation. The framework atoms were fixed, and four trial moves for CO_2 (displacement, rotation, creation, and deletion) were made with the same probabilities. The system was equilibrated for 1×10^7 Monte Carlo steps, after which data were collected for another 1×10^7 steps. The length of the Markov chain of 1×10^7 steps corresponds to more than 6×10^4 trials per CO_2. The simulation box for each temperature was constructed with $3 \times 3 \times 2$ unit cells, and periodic boundary conditions were applied in *a*, *b*, and *c* directions.

The guest–guest and guest–host interaction potential, U_{guest}, was assumed to be the sum of the Coulombic and Lennard-Jones (LJ) potentials:

$$U_{\text{guest}} = U_{\text{Coulombic}} + U_{\text{LJ}}, \quad (1)$$

$$U_{\text{Coulombic}} = \sum \frac{q_i q_j}{4\pi\varepsilon_0 r_{ij}}, \quad (2)$$

$$U_{\text{LJ}} = \sum 4\varepsilon_{ij}\left[\left(\frac{\sigma_{ij}}{r_{ij}}\right)^{12} - \left(\frac{\sigma_{ij}}{r_{ij}}\right)^{6}\right], \quad (3)$$

where q_i is the atomic charge, ε_0 (= 8.8542×10^{-12} $C^2 \cdot N^{-1} \cdot m^{-2}$) is the vacuum permittivity, r_{ij} is the interatomic distance, and σ_{ij} and ε_{ij} are the LJ parameters. The Ewald summation method was used to correct the long-range Coulombic interactions with a charge screening constant of 2.0 nm^{-1} and the reciprocal space sum for $\boldsymbol{k}$ vectors of $L_a/2\pi|\boldsymbol{k}|$, $L_b/2\pi|\boldsymbol{k}|$, and $L_c/2\pi|\boldsymbol{k}| \leq 10$ (where L_a, L_b, and L_c are the lengths of each of the simulation boxes). The short-range interactions were calculated with the cross interaction parameters obtained from the Lorentz-Berthelot mixing rules, and were truncated at a cut-off distance of 1.6289 nm (<0.5 min(L_a, L_b, L_c)). The atomic charges in each of the host frameworks were obtained by periodic density functional theory (DFT) calculations at the GGA-PBE/DNP level and Mulliken population analysis using the DMol^3 package.[42,43] In the DFT calculation, a primitive cell was chosen to reduce the computational cost. The modified universal force field (UFF)[44] , which was optimized for ELM-11 in our previous work, as σ_{UFF} and $0.74\varepsilon_{UFF}$,[24] was applied to the framework atoms to calculate the LJ interaction term. The parameters for the CO_2–CO_2 interaction (the atomic charges and the LJ parameters for carbon and oxygen, and the C–O bond length) were adopted from Chen *et al.*[45] (see Table S1, ESI†).

Free energy analysis

The osmotic free energy of a system in *i* state, Ω_i^{OS}, is given by[11]

$$\Omega_i^{\text{OS}}\left(N_i^{\text{host}}, \mu, P, T\right) = F_i^{\text{host}}\left(N_i^{\text{host}}, V_i, T\right) + PV_i + \Omega_i^{\text{guest}}\left(\mu, V_i, T\right), \quad (4)$$

where N_i^{host} is the number of host framework atoms, μ is the chemical potential of the adsorbed guest and the external gas, *P* is the external gas pressure at μ, *T* is the temperature, F_i^{host} is the Helmholtz free energy of the host, V_i is the volume of the host, and Ω_i^{guest} is the grand potential of the guest. The grand potential can be calculated by integrating a fictitious adsorption isotherm of a guest on the host framework at the *i* state, N_i^{guest}, as

$$\Omega_i^{\text{guest}}\left(\mu, V_i, T\right) = -k_{\text{B}} T N_i^{\text{guest}}\left(\mu_{\text{id}}, V_i, T\right) - \int_{\mu_{\text{id}}}^{\mu} N_i^{\text{guest}}\left(\mu', V_i, T\right) d\mu', \quad (5)$$

where k_B is the Boltzmann constant. The first term on the right-hand side is the grand potential at a sufficiently small chemical potential, μ_{id}. The osmotic free energy difference between the open state and the closed state, $\Delta\Omega^{OS}$, is represented as

$$\begin{aligned}\Delta\Omega^{\text{OS}} &= \Omega_{\text{op}}^{\text{OS}}\left(N_{\text{op}}^{\text{host}}, \mu, P, T\right) - \Omega_{\text{cl}}^{\text{OS}}\left(N_{\text{cl}}^{\text{host}}, \mu, P, T\right) \\ &= F_{\text{op}}^{\text{host}}\left(N_{\text{op}}^{\text{host}}, V_{\text{op}}, T\right) - F_{\text{cl}}^{\text{host}}\left(N_{\text{cl}}^{\text{host}}, V_{\text{cl}}, T\right) + P\left(V_{\text{op}} - V_{\text{cl}}\right) \cdot \\ &\quad + \Omega_{\text{op}}^{\text{guest}}\left(\mu, V_{\text{op}}, T\right) - \Omega_{\text{cl}}^{\text{guest}}\left(\mu, V_{\text{cl}}, T\right)\end{aligned} \quad (6)$$

The subscripts 'op' and 'cl' denote the open state and the closed state, respectively. When the grand potential of the closed state is zero independently of μ because of the absence of guest adsorption, eqn (6) can be rewritten as a function of μ and *T* as

$$\Delta\Omega^{\text{OS}}\left(\mu, T\right) = \Delta F^{\text{host}}(T) + P(\mu)\Delta V + \Omega_{\text{op}}^{\text{guest}}\left(\mu, T\right), \quad (7)$$

where ΔF^{host} is the Helmholtz free energy change required to deform the host framework from the closed state to the open state. ΔV is the volume change of the host, and the $P\Delta V$ term is negligible in most cases. $\Delta\Omega^{OS}$ should be zero at the chemical potential of the equilibrium gate adsorption, μ_{gate}, and therefore, the following equation is derived from eqn (5) and (7).

$$\Delta F^{\text{host}}(T) - k_{\text{B}} T N_{\text{op}}^{\text{guest}}\left(\mu_{\text{id}}, T\right) - \int_{\mu_{\text{id}}}^{\mu_{\text{gate}}} N_{\text{op}}^{\text{guest}}\left(\mu', T\right) d\mu' = 0 \quad (8)$$

The thermodynamic relation of ΔF^{host} is then expressed as

$$\Delta F^{\text{host}}(T) = \Delta U^{\text{host}}(T) - T\Delta S^{\text{host}}(T), \quad (9)$$

where ΔU^{host} and ΔS^{host} are differences in the internal energy and entropy between the closed and open host framework structures. In this study, we determined ΔU^{host} and ΔS^{host} by the following procedure. First, we calculated the fictitious adsorption isotherms of CO_2 on the open framework structures at each temperature (195–298 K) by the GCMC method. Then, the ΔF^{host} values at the respective temperatures were obtained by integrating the GCMC isotherms from μ_{id} to μ_{gate} according to eqn (8), and finally ΔU^{host} and ΔS^{host} were extracted from the obtained temperature dependence of ΔF^{host} according to eqn (9).

Note that the experimental adsorption isotherms of CO_2 on ELM-11 at 195–298 K show a hysteresis loop resulting from the difference in the gate adsorption and desorption pressures. In a previous work, we found that the desorption branch is close to the thermodynamic equilibrium transition pressure by conducting the free energy analysis for the simplified SPC model with a stacked-layer structure.[18] We therefore used μ_{gate} converted from the experimental gate desorption pressure.

Dispersion-corrected DFT calculation

The internal energy of the host, U^{host}, can be represented as the sum of the total potential energy of the host, u^{host}, and the kinetic energy of the host, K^{host}. If the kinetic energy of the

closed structure is comparable with that of the open structure at the same temperature, ΔU^{host} is approximated as

$$\Delta U^{host} = \Delta u^{host} + \Delta K^{host} \approx \Delta u^{host} = u_{op}^{host} - u_{cl}^{host}, \quad (10)$$

where u_{op}^{host} and u_{cl}^{host} are the internal energy of the open and closed host framework structures, respectively. The u_{op}^{host} and u_{cl}^{host} values were obtained by dispersion-corrected DFT (DFT-D) calculations with periodic boundary conditions using the VASP package.[46,47] Projector-augmented wave method pseudoptentials[48] with the GGA-PBE exchange-correlation functional and 400 eV plane wave cut-offs were used. We tested DFT-D2,[49] DFT-D3,[50] DFT-D3(BJ),[51] and Tkatchenko-Scheffler method (DFT-TS)[52] to correct London dispersion interactions, which are available on the VASP package.

It is possible that the host framework structure obtained from the Rietveld analysis has energetically unfavourable distortions because only the goodness of fit between the observed and calculated XRPD diagrams is taken into consideration in the analysis. Therefore, before the evaluation of the u_{op}^{host} and u_{cl}^{host} values, we conducted geometry optimizations of the open and closed host framework structures at 273 K obtained from the Rietveld analysis. The lattice constant of the host was fixed during the optimization, and atomic relaxation was performed until the force on all the atoms was lower than 0.1 eV/nm. The open host framework structure was relaxed in the presence of adsorbed CO_2 molecules, and then u_{op}^{host} was obtained by the single-point energy calculation using the optimized structure from which adsorbed CO_2 molecules were removed.

Results and discussion

Structural analysis using X-ray powder diffraction data

The XRPD patterns of ELM-11 in the open and closed states are shown in Fig. 1. The distinctive difference between the XRPD patterns at each state suggests that the host framework deforms dramatically because of the CO_2 adsorption. Meanwhile, the increase in temperature does not bring significant changes to the XRPD patterns, though some peaks such as $20\bar{2}$ (open) or 202 (closed) are slightly shifted to lower diffraction angles. The resulting Rietveld refinement patterns and structural models of ELM-11 ⊃ $2CO_2$ at 195–298 K are shown in Fig. S1–S3, ESI†, and the obtained crystallographic parameters are tabulated in Table 1 and Tables S2–S5, ESI†. These results indicate that the distance between the 2D-square-grid layers, which is calculated from the $(20\bar{2})$ lattice spacing, slightly increases by 2.2% when the temperature is increased from 195 K to 298 K; however, coordinates of atoms in the layer remain nearly unchanged with temperature. The resulting Rietveld refinement pattern at 273 K and Le Bail fitting patterns at 195–248 and 298 K of ELM-11 in the closed state are shown, respectively, in Fig. 2 and Fig. S4, ESI†, and their corresponding crystallographic parameters are tabulated in Table 2 and Table S6, ESI†, respectively. The obtained cell parameters are in good agreement with those reported by Bon *et al.*[36] The interlayer distance corresponding to the (202) lattice spacing increases by 1.3% from 195 K to 298 K, but the skeleton of the layer probably does not change compared with that of the open structure.

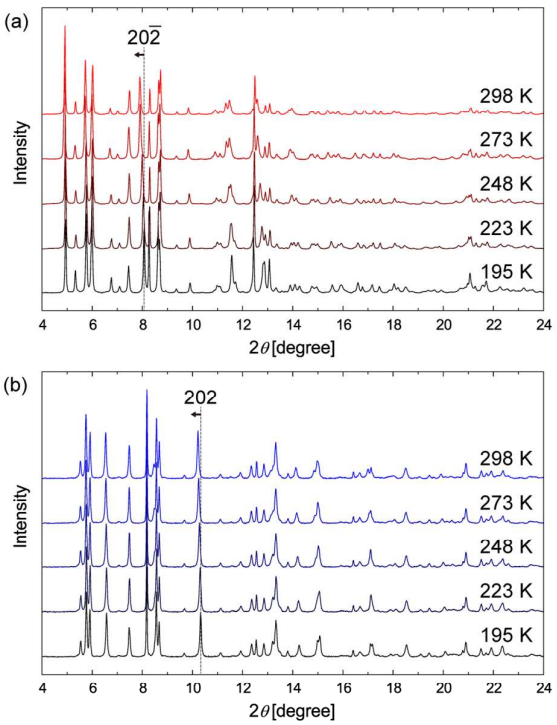

Fig. 1 Temperature dependence of XRPD patterns for (a) ELM-11 ⊃ $2CO_2$ and (b) ELM-11. Background is removed for all the XRPD patterns.

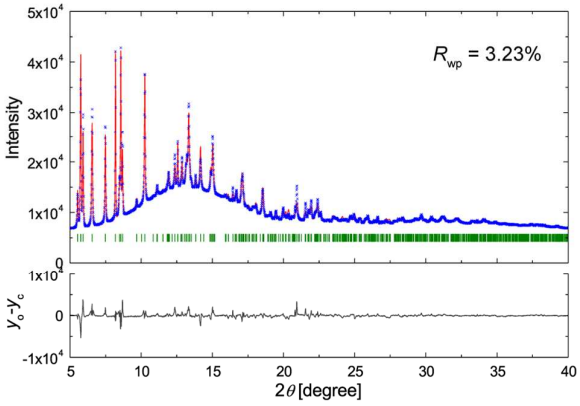

Fig. 2 Rietveld refinement XRPD pattern of ELM-11 at 273 K. The bottom panel shows the residual error.

Structural changes induced by guest adsorption

We compared the closed and open structures of ELM-11 obtained from the Rietveld refinement to understand how the host framework deforms during CO_2 adsorption. Fig. 3 shows the skeleton of one 2D-square-grid layer in the open state (parallel to an x-y plane), which is overlapped with that in the closed state. It is clear that rearrangement of the coordination

bond is not caused by gate-opening, though the orientations of the pyridine ring of a bpy molecule and the BF_4 anions are slightly changed. Fig. 4 shows how 2D-square-grid layers are stacked in each state. ELM-11 exhibits a 30% increase (0.446–0.578 nm) in the interlayer distance by encapsulating CO_2 molecules instead of gliding the layers to x and/or y directions. As shown in Fig. 5, at the closed state, two BF_4^- anions attached to the upper (yellow) and lower (black) layers occupy

a space of one square grid in the middle (red) layer composed of four bpy molecules. We found that the gate adsorption of CO_2 occurred owing to the generation of a void inside a square grid of the layer, which is caused by withdrawal of the BF_4^- anions with the widening of the interlayer distance. It is worth noting that the interlayer spacing of the open state is not large

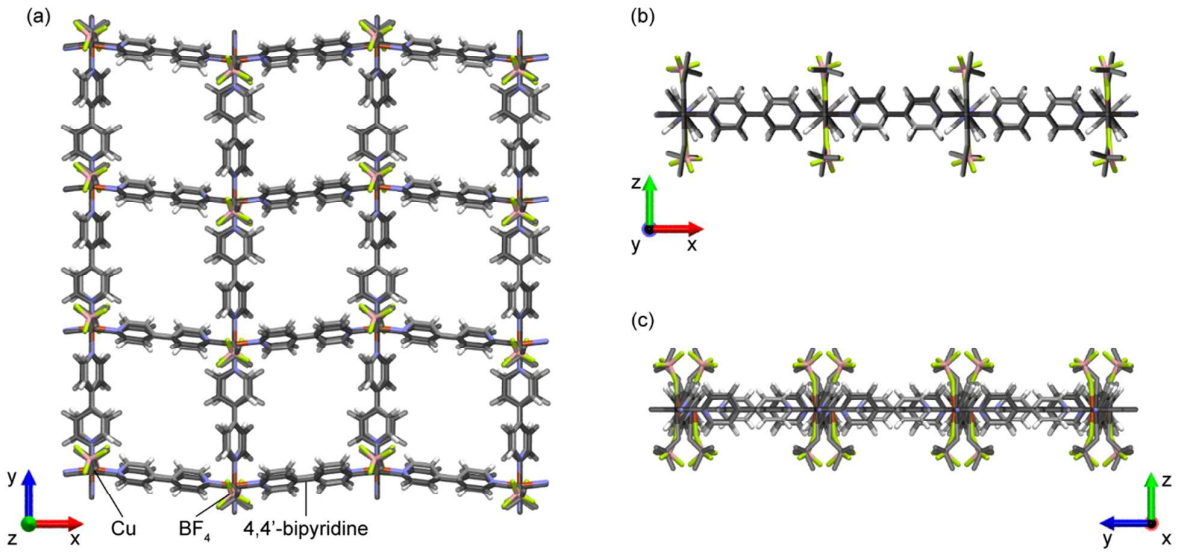

Fig. 3 Comparison of the structures of 2D-square grid layer of ELM-11 ⊃ $2CO_2$ (full colour) and ELM-11 (grey scale): (a) top view (x-y plane), (b) side view (x-z plane), and (c) side view (y-z plane).

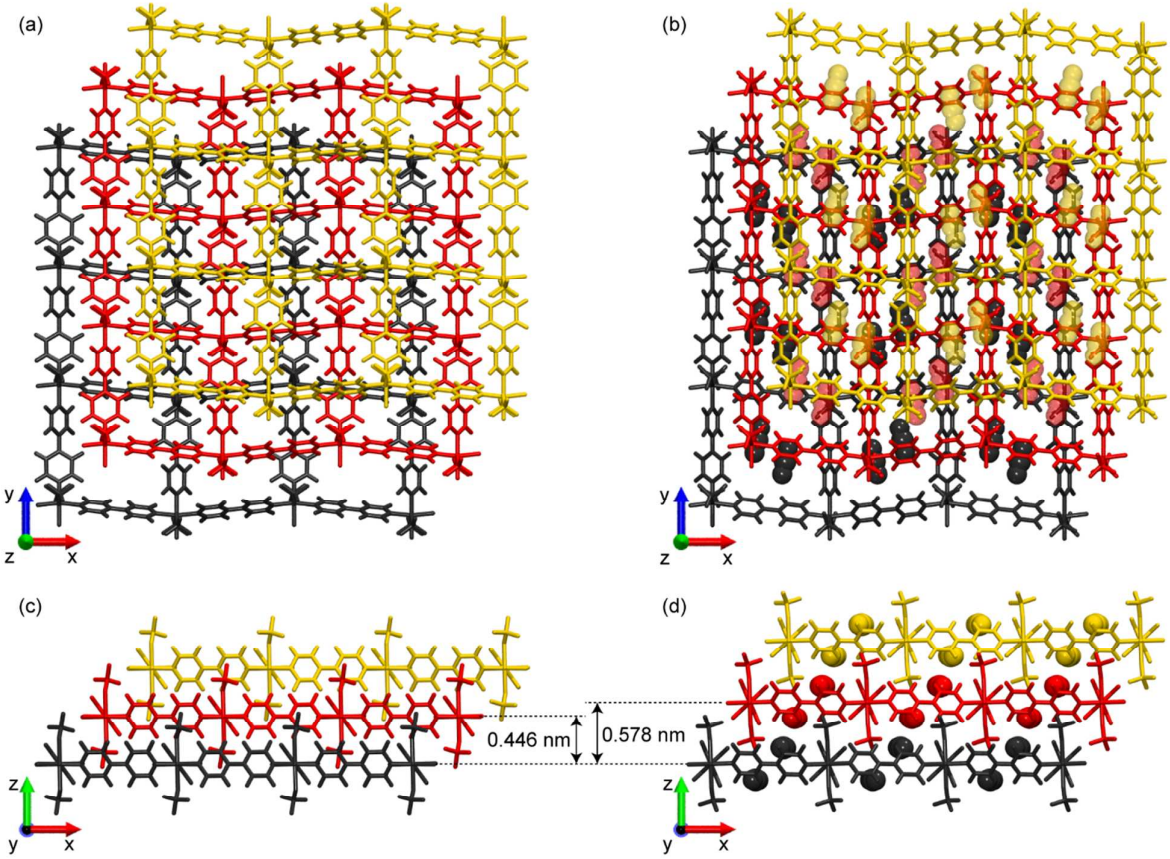

Fig. 4 Snapshots of ELM-11 before and after the gate adsorption: (a) top view of the closed state, (b) top view of the open state, (c) side view of the closed state, and (d) side view of the open state. All atoms belonging to one 2D-square grid layer have the same colour.

enough for a CO_2 molecule to pass through; however, 1D channels composed of the stacked square grids are formed after the expansion, as demonstrated in Fig. 6, which suggests that CO_2 molecules penetrate through the 1D channels.

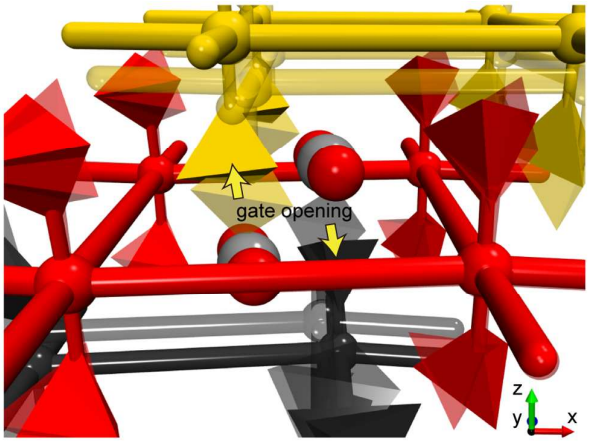

Fig. 5 Schematic representation of the gate opening of ELM-11 induced by CO_2 adsorption. Translucent and non-transparent materials are the host frameworks before and after the gate opening. The Cu atom is represented by a sphere and the BF_4 and bpy molecules are represented by a trigonal pyramid and a rod, respectively.

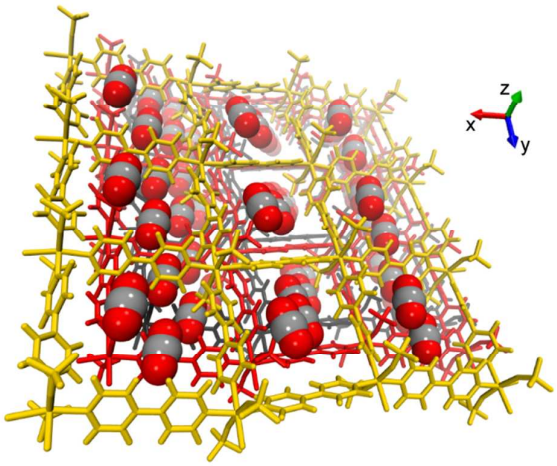

Fig. 6 Snapshot of 1D channels encapsulating CO_2 molecules.

Free energy analysis

The atomic charges in the open host frameworks at 195–298 K were determined by the DFT calculations and Mulliken population analysis, and the data are tabulated in Table S7, ESI†. It is often claimed that a disadvantage of Mulliken population analysis is that it depends strongly on the basis set used;[53,54] however, in a previous work,[24] we confirmed that the ELM-11–CO_2 interaction potential can be appropriately calculated using the Mulliken charges and by comparing the results with those obtained from the ab initio calculation. Fig. 7a shows the fictitious adsorption isotherms of CO_2 simulated by GCMC at 195–298 K together with the experimental adsorption isotherms. At higher pressure than the experimental gate adsorption pressure, the simulated

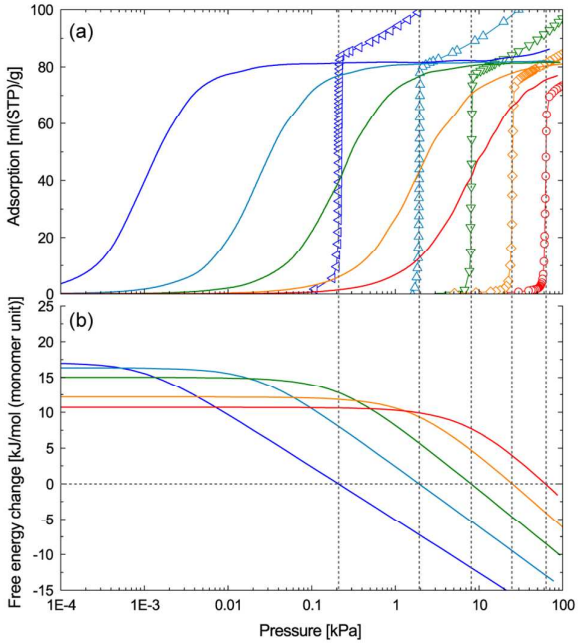

Fig. 7 (a) Fictitious adsorption isotherms of CO_2 on the open host framework structures of ELM-11 at 195 (blue), 223 (cyan), 248 (green), 273 (orange), and 298 K (red) simulated by GCMC (lines) and experimental adsorption isotherms (lines with markers). (b) Osmotic free energy changes of system $\Delta\Omega^{OS}$.

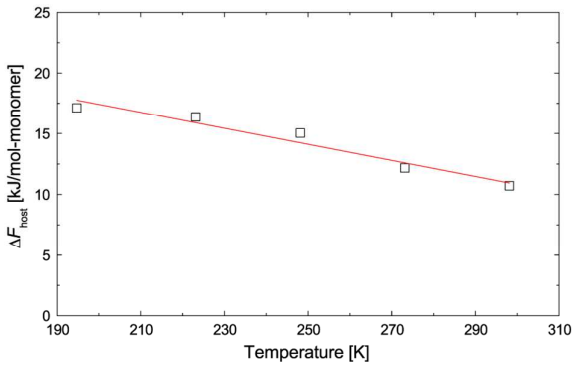

Fig. 8 Temperature dependence of the Helmholtz free energy change of host ΔF_{host} obtained from the free energy analysis. The red line is least-squares fitting of eqn (9) assuming that ΔU^{host} and ΔS^{host} are temperature-independent parameters.

adsorption amount tends to become smaller than that obtained experimentally; this phenomenon is noticeable at low temperatures. This suggests that further loadings of CO_2 occur with the reorientation of BF_4^- anions for real ELM-11. In fact, we found that three CO_2 molecules per monomer unit could be encapsulated in the rigid open host framework at low temperatures and/or high pressures by GCMC (see Fig. S5, ESI†). The implementation of a trial move of BF_4^- in GCMC would solve the mismatch; however, in order to perform the free energy analysis, the GCMC isotherm has to coincide only

Table 3 Internal energy change of the host framework of ELM-11.

Method of calculation	u_{op}^{host} [kJ/mol*]	u_{cl}^{host} [kJ/mol*]	Δu_{DFT} [kJ/mol*]	$\Delta u_{dispersion}$ [kJ/mol*]	ΔU^{host} (= $\Delta u_{DFT} + \Delta u_{dispersion}$) [kJ/mol*]	ΔS^{host} [J/mol*·K]
DFT-D2[49]	–32404.98	–32448.20	–29.56	72.78	43.22	–
DFT-D3[50]	–32344.15	–32376.22	–28.00	60.07	32.07	–
DFT-D3(BJ)[51]	–32427.75	–32459.98	–28.13	59.36	31.23	–
DFT-TS[52]	–32342.90	–32391.40	–28.16	76.66	48.50	–
Free energy analysis	–	–	–	–	30.6	65.9

* monomer unit: $Cu(bpy)_2(BF_4)_2$.

with the experimentally adsorbed amount immediately after gate adsorption. The grand thermodynamic potentials of guest Ω_{op}^{guest} at 195–298 K were calculated by integrating the fictitious adsorption isotherms. Fig. 7b shows the free energy changes of system $\Delta\Omega^{OS}$ at each temperature, which were obtained by shifting the Ω_{op}^{guest} profiles so that $\Delta\Omega^{OS}$ becomes zero at the corresponding experimental gate adsorption pressure. The Helmholtz free energy changes of host ΔF^{host} at 195–298 K, which are equivalent to the $\Delta\Omega^{OS}$ values at P = 0, were obtained by applying eqn (8). It is clear from Fig. 8 that there is a linear correlation between ΔF^{host} and temperature, which suggests that the temperature dependence of the internal energy and entropy changes of host, ΔU^{host} and ΔS^{host}, respectively, are negligibly small according to eqn (9). We thus obtained ΔU^{host} = 30.6 kJ/mol-monomer and ΔS^{host} = 65.9 J/K·mol-monomer by the least-squares fitting of eqn (9) by assuming that ΔU^{host} and ΔS^{host} are temperature-independent parameters.

Dispersion-corrected DFT calculation

The closed and open host framework structures determined from the in situ synchrotron XRPD patterns at 273 K were optimized by the DFT-D calculation, and the obtained internal energies, u_{cl}^{host} and u_{op}^{host}, are tabulated in Table 3. It is clear that the deformation of the host framework increases the non-bonded interaction energy ($u_{dispersion}$) and decreases the bonded potential energy (u_{DFT}). The decrease in u_{DFT} indicates that the skeleton of 2D-square-grid layer was stabilized after the widening of the interlayer distance, mainly because the distorted coordination bonds between Cu and bpy molecules were relaxed. The obtained internal energy changes of host ΔU^{host} (= $u_{op}^{host} - u_{cl}^{host}$) are in the range of 31.23–48.50 kJ/mol-monomer, depending on the dispersion correction method, and the ΔU^{host} values are close to ΔU^{host} = 30.6 kJ/mol-monomer obtained from the free energy analysis. In particular, the errors between the ΔU^{host} values from the free energy analysis and the DFT-D calculations using DFT-D3 and DFT-D3(BJ) by Grimme *et al.*[50,51] are less than 5%. This fact demonstrates that the ΔF^{host} values obtained from the free energy analysis are supported by the ab initio calculations and thus the gate opening behaviour on the real SPCs can be well described by the thermodynamic model.

Note that the Cu–F bond lengths of the closed and open structures become long by ca. 0.03 nm after the geometry optimizations by DFT-D, as shown in Table S8, ESI†. This may be owing to the following reasons: the Rietveld analysis for ELM-11 should have a molecular-level resolution only, because the reflections at high angles are extensively overlapped; the DFT calculation is not always perfect because it depends on the exchange-correlation functionals and basis sets. We however confirmed that the change in the structure after the geometry optimization did not significantly affect the R_{wp} value and the adsorption amount of CO_2 by GCMC did not change at all, as demonstrated in Fig. S6 and S7, ESI†.

Conclusions

The structure of ELM-11 in the closed state was determined by our unique method, which combines the Rietveld analysis with molecular simulations. The comparison between the closed and open host framework structures of ELM-11 provides a detailed picture about the adsorption-induced structural transition: a void is generated inside a square grid of the ELM-11 layer due to the withdrawal of BF_4^- anions with the widening of the interlayer distance by 30%; as a result, a 1D channel composed of stacked square girds are formed and CO_2 molecules penetrate ELM-11 through the 1D channels.

We performed the GCMC simulations with the open framework structures at 195–298 K, and obtained the precise Helmholtz free energy changes of the host at each temperature by free energy analysis. The internal energy change of the host was determined from the temperature dependence of the Helmholtz free energy change of the host, which was in good agreement with that obtained by the DFT-D calculations using the closed and open host framework structures. Thus, we can conclude that the gate-opening behaviour of the real SPCs is described by the thermodynamic model. Note that, in our previous study, we roughly estimated the entropy change of host for CO_2 adsorption on ELM-11 in the temperature range 258–283 K and obtained ΔS^{host} = 56 J/K·mol-monomer, which differs somewhat from the value evaluated in this study (ΔS^{host} = 65.9 J/K·mol-monomer). This is probably because, in the present study, the temperature dependence of ΔF^{host} was determined by the free energy analysis over a wider temperature range (195–298 K) by using the open host framework structures refined by the Rietveld analysis at the corresponding temperature, while, in the previous work, it was estimated from the data over a narrower

temperature range (258–283 K) by only using the open host framework structure at 273 K neglecting its temperature dependence.

The future challenge is to establish a guideline for the tailored synthesis of SPCs on the basis of the thermodynamic model. Our results demonstrate that changes in both the internal energy and entropy of the host are important factors to control the gate adsorption pressure. This suggests that the gate adsorption pressure can be tuned not only by changing the guest-host and/or intra-host interaction potentials but also by modifying the functional group of the host with different degrees of freedom, which results in the change of the entropy term. Such a study is now in progress.

Acknowledgements

This work was financially supported by a Grant-in-Aid for JSPS Fellows No. 15J05846, a Grant-in-Aid for Young Scientists (A) No. 25709074, a Grant-in-Aid for Challenging Exploratory Research No. 26620060, and JST, CREST. The synchrotron radiation experiments were performed at the BL02B2 beamline of SPring-8 with the approval of the Japan Synchrotron Radiation Research Institute (JASRI) (Proposal No. 2014A1317, 2014B1110, 2015A1220, and 2015A1759). We thank Prof. Katsumi Kaneko, Prof. Hirofumi Kanoh, Dr. Atsushi Kondo, and Dr. Hiroshi Kajiro for fruitful discussions.

Notes and references

1 O. M. Yaghi and H. Li, *J. Am. Chem. Soc.*, 1995, **117**, 10401–10402.
2 O. M. Yaghi, G. Li and H. Li, *Nature*, 1995, **378**, 703–706.
3 S. Kitagawa and M. Kondo, *Bull. Chem. Soc. Jpn.*, 1998, **71**, 1739–1753.
4 M. Kondo, K. Fujimoto, T. Okubo, A. Asami, S. Noro, S. Kitagawa, T. Ishii and H. Matsuzaka, *Chem. Lett.*, 1999, 291–292.
5 S. L. James, *Chem. Soc. Rev.*, 2003, **32**, 276–288.
6 G. Férey, *Chem. Soc. Rev.*, 2008, **37**, 191–214.
7 S. Kitagawa, R. Kitaura and S. Noro, *Angew. Chem. Int. Ed. Engl.*, 2004, **43**, 2334–2375.
8 S. Kitagawa and K. Uemura, *Chem. Soc. Rev.*, 2005, **34**, 109–119.
9 S. Horike, S. Shimomura and S. Kitagawa, *Nat. Chem.*, 2009, **1**, 695–704.
10 W. Kosaka, K. Yamagishi, J. Zhang and H. Miyasaka, *J. Am. Chem. Soc.*, 2014, **136**, 12304–12313.
11 F.-X. Coudert, M. Jeffroy, A. H. Fuchs, A. Boutin and C. Mellot-Draznieks, *J. Am. Chem. Soc.*, 2008, **130**, 14294–14302.
12 A. Boutin, M.-A. Springuel-Huet, A. Nossov, A. Gédéon, T. Loiseau, C. Volkringer, G. Férey, F.-X. Coudert and A. H. Fuchs, *Angew. Chem. Int. Ed. Engl.*, 2009, **48**, 8314–8317.
13 F.-X. Coudert, C. Mellot-Draznieks, A. H. Fuchs and A. Boutin, *J. Am. Chem. Soc.*, 2009, **131**, 11329–11331.
14 A. V. Neimark, F.-X. Coudert, A. Boutin and A. H. Fuchs, *J. Phys. Chem. Lett.*, 2010, **1**, 445–449.
15 A. V. Neimark, F.-X. Coudert, C. Triguero, A. Boutin, A. H. Fuchs, I. Beurroies and R. Denoyel, *Langmuir*, 2011, **27**, 4734–4741.
16 S. Watanabe, H. Sugiyama, H. Adachi, H. Tanaka and M. T. Miyahara, *J. Chem. Phys.*, 2009, **130**, 164707.
17 H. Sugiyama, S. Watanabe, H. Tanaka and M. T. Miyahara, *Langmuir*, 2012, **28**, 5093–5100.
18 R. Numaguchi, H. Tanaka, S. Watanabe and M. T. Miyahara, *J. Chem. Phys.*, 2013, **138**, 054708.
19 R. Numaguchi, H. Tanaka, S. Watanabe and M. T. Miyahara, *J. Chem. Phys.*, 2014, **140**, 044707.
20 R. Numaguchi, H. Tanaka, S. Hiraide and M. T. Miyahara, *Mol. Simul.*, 2015, **41,** 1329–1338.
21 D. Bousquet, F.-X. Coudert and A. Boutin, *J. Chem. Phys.*, 2012, **137**, 044118.
22 D. Bousquet, F.-X. Coudert, A. G. J. Fossati, A. V. Neimark, A. H. Fuchs and A. Boutin, *J. Chem. Phys.*, 2013, **138**, 174706.
23 H. Tanaka, S. Ohsaki, S. Hiraide, D. Yamamoto, S. Watanabe and M. T. Miyahara, *J. Phys. Chem. C*, 2014, **118**, 8445–8454.
24 H. Tanaka, S. Hiraide, A. Kondo and M. T. Miyahara, *J. Phys. Chem. C*, 2015, **119**, 11533–11543.
25 D. Li and K. Kaneko, *Chem. Phys. Lett.*, 2001, **335**, 50–56.
26 S. Onishi, T. Ohmori, T. Ohkubo, H. Noguchi, L. Di, Y. Hanzawa, H. Kanoh and K. Kaneko, *Appl. Surf. Sci.*, 2002, **196**, 81–88.
27 H. Noguchi, A. Kondoh, Y. Hattori, H. Kanoh, H. Kajiro and K. Kaneko, *J. Phys. Chem. B*, 2005, **109**, 13851–13853.
28 A. Kondo, H. Noguchi, S. Ohnishi, H. Kajiro, A. Tohdoh, Y. Hattori, W.-C. Xu, H. Tanaka, H. Kanoh and K. Kaneko, *Nano Lett.*, 2006, **6**, 2581–2584.
29 H. Noguchi, A. Kondo, Y. Hattori, H. Kajiro, H. Kanoh and K. Kaneko, *J. Phys. Chem. C*, 2007, **111**, 248–254.
30 H. Kanoh, A. Kondo, H. Noguchi, H. Kajiro, A. Tohdoh, Y. Hattori, W.-C. Xu, M. Inoue, T. Sugiura, K. Morita, H. Tanaka, T. Ohba and K. Kaneko, *J. Colloid Interface Sci.*, 2009, **334**, 1–7.
31 H. Kajiro, A. Kondo, K. Kaneko and H. Kanoh, *Int. J. Mol. Sci.*, 2010, **11**, 3803–3845.
32 A. Kondo, H. Kajiro, H. Noguchi, L. Carlucci, D. M. Proserpio, G. Ciani, K. Kato, M. Takata, H. Seki, M. Sakamoto, Y. Hattori, F. Okino, K. Maeda, T. Ohba, K. Kaneko and H. Kanoh, *J. Am. Chem. Soc.*, 2011, **133**, 10512–10522.
33 Y. Cheng, H. Kajiro, H. Noguchi, A. Kondo, T. Ohba, Y. Hattori, K. Kaneko and H. Kanoh, *Langmuir*, 2011, **27**, 6905–6909.
34 A. Kondo, N. Kojima, H. Kajiro, H. Noguchi, Y. Hattori, F. Okino, K. Maeda, T. Ohba, K. Kaneko and H. Kanoh, *J. Phys. Chem. C*, 2012, **116**, 4157–4162.
35 J. Yang, Q. Yu, Q. Zhao, J. Liang, J. Dong and J. Li, *Microporous Mesoporous Mater.*, 2012, **161**, 154–159.
36 V. Bon, I. Senkovska, D. Wallacher, A. Heerwig, N. Klein, I. Zizak, R. Feyerherm, E. Dudzik and S. Kaskel, *Microporous Mesoporous Mater.*, 2014, **188**, 190–195.
37 M. Takata, E. Nishibori, K. Kato, Y. Kubota and M. Sakata, *Adv. X-ray Anal.*, 2002, **45**, 377–384.
38 *Rigaku J.*, 2010, **26**, 23–27.
39 F. Izumi and K. Momma, *Solid State Phenom.*, 2007, **130**, 15–20.
40 F. Izumi and K. Momma, *IOP Conf. Ser. Mater. Sci. Eng.*, 2011, **18**, 022001.
41 F. Izumi and T. Ikeda, *Mater. Sci. Forum*, 2000, **321–324**, 198–203.
42 B. Delley, *J. Chem. Phys.*, 1990, **92**, 508–517.
43 B. Delley, *J. Chem. Phys.*, 2000, **113**, 7756–7764.
44 A. K. Rappé, C. J. Casewit, K. S. Colwell, W. A. Goddard III and W. M. Skiff, *J. Am. Chem. Soc.*, 1992, **114**, 10024–10035.
45 Y. F. Chen, J. Y. Lee, R. Babarao, J. Li and J. W. Jiang, *J. Phys. Chem. C*, 2010, **114**, 6602–6609.
46 G. Kresse and J. Furthmüller, *Comput. Mater. Sci.*, 1996, **6**, 15–50.
47 G. Kresse and J. Furthmüller, *Phys. Rev. B*, 1996, **54**, 11169–11186.
48 P. E. Blöchl, *Phys. Rev. B*, 1994, **50**, 17953–17979.
49 S. Grimme, *J. Comput. Chem.*, 2006, **27**, 1787–1799.

50 S. Grimme, J. Antony, S. Ehrlich and H. Krieg, *J. Chem. Phys.*, 2010, **132**.
51 S. Grimme, S. Ehrlich and L. Goerigk, *J. Comput. Chem.*, 2011, **32**, 1456–1465.
52 A. Tkatchenko and M. Scheffler, *Phys. Rev. Lett.*, 2009, **102**, 6–9.
53 A. E. Reed, R. B. Weinstock and F. Weinhold, *J. Chem. Phys.*, 1985, **83**, 735–746.
54 J. J. Philips, M. A. Hudspeth, P. M. Browne and J. E. Peralta, *Chem. Phys. Lett.*, 2010, **495**, 146–150.